VOLUME 160 • ISSUE 3 • MARCH 2013

ELSEVIER

Combustion and Flame

THE JOURNAL OF THE COMBUSTION INSTITUTE

Available online at www.sciencedirect.com

SciVerse ScienceDirect

High temperature ignition delay times of C5 primary alcohols

Chenglong Tang [a,*], Liangjie Wei [a], Xingjia Man [a], Jiaxiang Zhang [a], Zuohua Huang [a,*], Chung K. Law [b]

[a] State Key Laboratory of Multiphase Flows in Power Engineering, Xi'an Jiaotong University, Xi'an 710049, People's Republic of China
[b] Department of Mechanical and Aerospace Engineering, Princeton University, Princeton, NJ 08540-5263, United States

ABSTRACT

Ignition delay times of the three C5 primary alcohol isomers (*n*-pentanol, *iso*-pentanol and 2-methyl-1-butanol) were measured behind reflected shock waves. Experiments were conducted in the temperature range of 1100–1500 K, pressures of 1.0 and 2.6 atm, equivalence ratios of 0.25, 0.5 and 1.0, and O_2 concentration in the fuel/O_2/Ar mixtures varying from 3.75% to 15%. Measurements show that the ignition delay time and the global activation energy of the three isomers both decrease in the order of *iso*-pentanol, 2-methyl-1-butanol, and *n*-pentanol. Chemical kinetic mechanisms for *n*-pentanol (Mech NP) and *iso*-pentanol (Mech IP), recently developed by Dagaut and co-workers, were used to model the respective ignition delay times. Results show that Mech NP yields close agreement at the equivalence ratio of 0.25, but the agreement is moderated with increasing equivalence ratio. Mech IP yields fairly close agreements at relatively higher temperatures but over-predicts the measurements by 50% at relatively lower temperatures for the three equivalence ratios studied. A new 2-methyl-1-butanol high temperature mechanism was proposed and validated against the ignition delay data. Sensitivity analysis for both *n*-pentanol and *iso*-pentanol showed the dominance of small radical reactions. Reaction pathway analysis aided further scrutiny of the fuel-specific reactions in Mech NP, leading to refinement of the kinetic model, and improved agreement between the predicted and measured ignition delay times as well as the jet-stirred reactor results.

© 2012 The Combustion Institute. Published by Elsevier Inc. All rights reserved.

1. Introduction

In response to the global concerns for greenhouse gas emissions and energy sustainability, biofuels have attracted increasing interests because of their renewability, reduction of greenhouse gas emissions [1], inhibition of PAH and soot formation [2], and domestic availability [3]. Bio-ethanol is the most widely used biofuel, being responsible for over 90% of the total biofuel production worldwide [4]. Consequently, extensive studies on ethanol have been conducted, including those on engine performances, emission characteristics [5,6], as well as fundamental data [7–9]. However, its volumetric energy density is only 35% of that of gasoline. Furthermore, ethanol is highly hygroscopic, and as such is corrosive to the fuel pipelines. For these reasons, recent research focus has shifted to C3 and C4 alcohols and their isomers. In particular, effects of C4 alcohol blending on the thermo performances and emission results of spark ignition engines [10,11], direct injection engines [12], and HCCI engines [13] have been investigated and the results show that C4 alcohol blending potentially facilitates cleaner and more efficient burning. In terms of fundamental

combustion, intermediate species concentrations in low-pressure, burner-stabilized isomeric C3 [14,15] and C4 [16,17] alcohol flames and *iso*-pentanol flames [18] have been studied using flame sampling molecular beam mass spectrometry techniques, yielding useful insights into the combustion chemistry of higher alcohols. Furthermore, laminar flame speed [19–21], ignition delay time [22–27], and flow reactor [28–31] data for these alcohols have also been collected for validation of kinetic mechanisms.

Significantly less work, however, has been conducted on C5 and higher alcohols. Recently, bio-synthesis of pentanol isomers in metabolically engineered microorganisms has been realized [32–34]. Though the commercial production of C5 alcohol has yet to be achieved, several engine and fundamental studies have already been conducted. Specifically, Yang et al. [35] stated that *iso*-pentanol (3-methyl-1-butanol) has great potential as an HCCI engine fuel because their experiments at low engine speeds did not show the two-stage ignition behavior, which typically occurs in gasoline engines. In addition, *iso*-pentanol shows comparably high intermediate-temperature heat release rate (ITHR) as gasoline, which facilitates HCCI operation without knock at high loads. Subsequently, Tsujimura et al. [36] developed a detailed kinetic mechanism for modeling the HCCI combustion with *iso*-pentanol, which reproduced the relationship between HCCI engine performances and engine operating conditions. Regarding fundamental

---

* Corresponding authors. Fax: +86 29 82668789.
E-mail addresses: chenglongtang@mail.xjtu.edu.cn (C. Tang), zhhuang@mail.xjtu.edu.cn (Z. Huang).

combustion, Togbe et al. [4] measured the concentration profiles of the stable species for *n*-pentanol oxidation in a jet-stirred reactor (JSR) at 10 atm and the laminar flame speeds of *n*-pentanol/air mixtures at 1.0 atm. Additionally, they developed a detailed kinetic mechanism (Mech NP) for *n*-pentanol oxidation, which show good agreement with the experimental results. As a follow-on study, Dayma et al. [37] conducted both experimental and kinetic study (Mech IP) of *iso*-pentanol oxidation in JSR, and good agreement between the proposed mechanism and experimental data was observed.

The motivation for the present study arises from the growing interest in higher alcohols as alternative fuels and the need for fundamental kinetics data for the development of the reaction mechanisms. In this study, shock-tube ignition delay times of the three C5 liquid primary alcohols, namely *n*-pentanol (ᴵ⌒⌒⌒ₒₕ), *iso*-pentanol (⌐₋ₒₕ) and 2-methyl-1-butanol (⌐₋ₒₕ) were, for the first time, measured. In the following, both experimentation and presentation of the ignition delay times, which are correlated as a function of the experimental parameters will be provided. Since the only available kinetic mechanisms for *n*-pentanol and *iso*-pentanol are those developed by Dagaut and co-workers [4,37], thus these kinetic mechanisms will be used to model the ignition delay times for comparison with the experimental measurements. Sensitivity analysis and reaction pathway analysis were also performed for both *n*-pentanol and *iso*-pentanol at selected conditions, and refinements of the fuel specific reactions in the mechanism are suggested.

2. Experimental and kinetic model specifications

2.1. Setup and procedures

The present shock-tube was an updated version of an earlier one described in Ref. [38]. Briefly, the shock tube (inner diameter 11.5 cm) consists of the driver section (2 m long) and the driven section (7.3 m long). In between them there is a connecting flange (0.06 m long) with diaphragms on both sides to separate the driver and reactant mixtures. The rupture of the diaphragm is triggered by evacuating the small volume of the flange section. Reactant mixtures are prepared in a stainless steel mixing tank. For all test conditions, the partial pressure of the fuel is assured to be less than 1/3 of its saturated vapor pressure at the tank temperature so as to exclude fuel condensation. Three liquid C5 primary alcohols, *n*-pentanol (99.5%), *iso*-pentanol (99.5%) and 2-methyl-1-butanol (99.5%), are used as the fuel. The purity of the gases used for the mixture preparation is of research grade (>99.95%).

Four piezoelectric pressure transducers (PCB 113B26) are installed in series along the last 1.5 m of the driven section, the signals of which are then sent to three time counters (Fluke PM6690) for determination of the shock wave velocities. The three velocities are linearly extrapolated to the shock tube endwall to determine the incident shock velocity, v_e, at the endwall. Initial temperature, initial pressure p_1, thermodynamic properties of the reactant (from Burcat and Ruscic [39]) mixtures and v_e are used as the input data for computing the reflected shock conditions (p, T) through one-dimensional shock relations. On the endwall, another piezoelectric pressure transducer (PCB 113B03) was mounted for measuring p. Additionally, a quartz-glass window (60 mm thick) together with a 430 nm narrow band pass filter and a photomultiplier (Hamamatsu, CR131) are mounted, through which the CH* emission is captured.

2.2. Ignition delay time definition and system validation

Figure 1a shows the typical reflected shock pressure p and recorded CH* emission history. It can be seen that upon ignition,
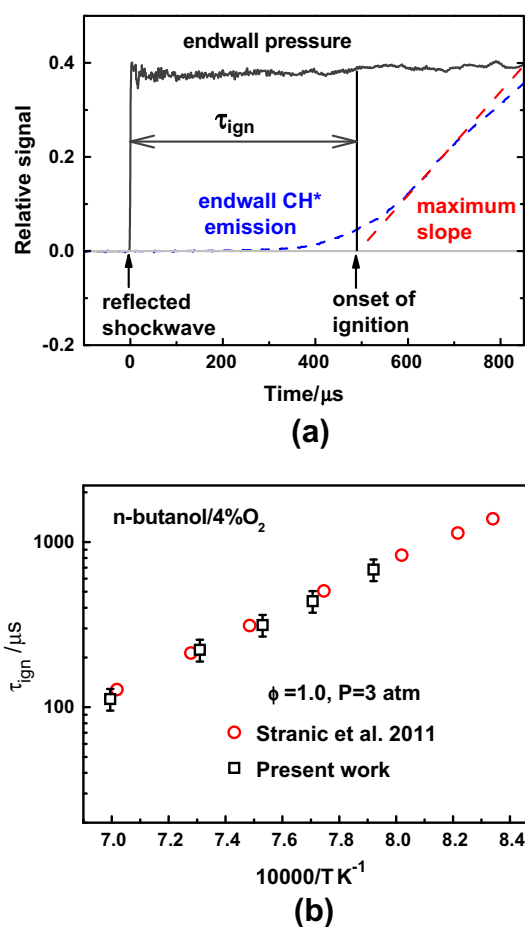

Fig. 1. (a) Typical endwall pressure and CH* emission signals and definition of ignition delay time and (b) comparison between present measurement and Stanford shock-tube results at 3 atm for ϕ = 1.0 *n*-butanol and 4% O₂ concentration diluted in Ar.

the pressure increase is very weak but a steep increase in the CH* emission is presented, thus the onset of ignition is defined by extrapolating the maximum slope of the CH* emission signal to the baseline and the ignition delay time τ_{ign} is consequently defined as the time between the arrival of the reflected shock wave and the onset of ignition. This definition has been extensively adopted in the previous shock-tube studies [24] for test conditions under which the onset of ignition could not be well defined in the case of weak pressure rise. The ignition delay time measurements have an uncertainty of 10% and that in the temperature calculation is about 25 K.

To validate the present measurement system and data processing procedure, ignition delay times of *n*-butanol/O₂/Ar was measured and compared with the measurements by Stranic et al. [24] under exactly the same test condition, as shown in Fig. 1b. Excellent agreement between the two data sets was given; thus the experimental data from the shock tube are reliable. The test conditions are summarized in Table 1.
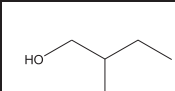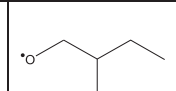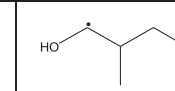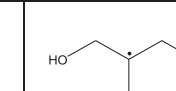
2.3. Kinetic model for numerical predictions
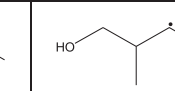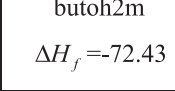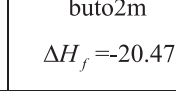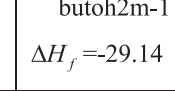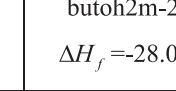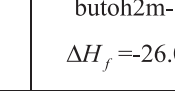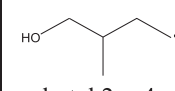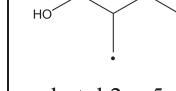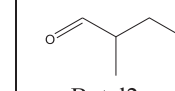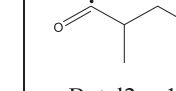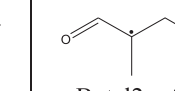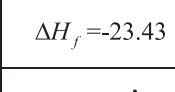
The ignition delay times of *n*-pentanol and *iso*-pentanol were computed using their available kinetic mechanisms, say Mech NP by Togbe et al. [4] and Mech IP by Dayma et al. [37]. As there is no available 2-methyl-1-butanol chemical kinetic mechanism (Mech 2M1B), we have attempted to build a high temperature

Table 1
Ignition delay time test conditions for *n*-pentanol, *iso*-pentanol and 2-methyl-1-butanol.

Test No.	Initial pressure p (atm)	Fuel concentration X_{Fuel} (%)	Oxygen concentration (%)
1	1.0	0.5	7.5
2	1.0	0.5	3.75
3	1.0	0.5	15
4	1.0	0.25	3.75
5	2.6	0.25	3.75

2-methyl-1-butanol mechanism, which consists of 1763 reactions and 283 species. The thermodynamic data for the new species in Mech 2M1B were computed by the THERM program of Ritter and Bozzelli [40] based on the group additivity methods in Ref. [41]. Since there have been no measured rate constants for the primary reactions of 2-methyl-1-butanol, we have then built up the sub-mechanism of 2-methyl-1-butanol based on a detailed *n*-butanol high temperature mechanism in our previous work [42]. The structures of the fuel related species were given in Table 2. The unimolecular decomposition of 2-methyl-1-butane includes the C–C bond rupture and the water elimination reactions. Most of the rate constants of H-abstractions by small species X (X = H, O, OH, CH₃, etc.) from the α site and OH group are taken from the *iso*-butanol mechanism [43,44] and abstraction from other sites are evaluated with the analogy of alkanes [45]. The subsequent fuel radicals are decomposed through β scission and the isomerization (rate constants estimated by using Reaction Mechanism Generator developed by P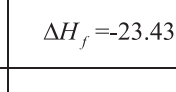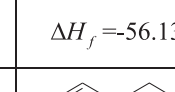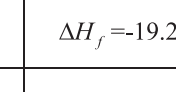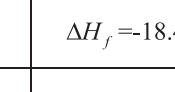rof. Green's group [46]) of the fuel radicals are also considered. Evaluation of rate constants of the above reactions, together with the thermodynamic data in Chemkin format, are available in the Supplementary material.

3. Results and discussions

The raw ignition delay time data are provided as Supplementary material. Through regression analysis, the raw ignition delay time (τ_{ign}, in μs) data for each isomer were correlated as a function of pressure (p, in atm), fuel mole fraction (X_{Fuel}), oxygen mole fraction (X_{O2}) and temperature (T, in K) in the following format:

$$\tau_{ign} = Ap^{-B}X_{Fuel}^{C}X_{O2}^{-D} \exp(E_a/RT) \tag{1}$$

where $R = 1.986 \times 10^{-3}$ kcal/(mole K) is the universal gas constant, and E_a is the global activation energy in kcal/mol. The correlation parameters are given in Table 3.

3.1. Ignition delay times: measurements and correlations

Figure 2 shows the measured ignition delay time as a function of temperature for *n*-pentanol (a), *iso*-pentanol (b) and 2-methyl-1-butanol (c). Under all test conditions, the measured ignition delay time exhibits a clear Arrhenius dependence on temperature, as expected. Furthermore, the ignition delay time increases with increasing equivalence ratio. The correlation of Eq. (1) shows very little deviation with the measured values, with r^2 values above 0.99 for all three fuels investigated. The experimental data in Fig. 2 were obtained for 0.5% fuel mole fraction and 1.0 atm pressure, for all three fuels. The ignition delay time versus pressure and oxygen concentration are not presented because Eq. (1) has already illustrated the negative dependence of τ_{ign} on p and X_{O2}. It is noted that since the ranges of pressure, oxygen concentration and equivalence ratio studied in this work are relatively small, Eq. (1) should not be used in conditions that deviate too much from those of the present work.

Table 2
Structures and heat of formation at 298 K of new species in Mech 2M1B (unit for ΔH_f is kcal/mol).

butoh2m ΔH_f=-72.43	buto2m ΔH_f=-20.47	butoh2m-1 ΔH_f=-29.14	butoh2m-2 ΔH_f=-28.03	butoh2m-3 ΔH_f=-26.08
butoh2m-4 ΔH_f=-23.43	butoh2m-5 ΔH_f=-23.43	Butal2m ΔH_f=-56.13	Butal2m-1 ΔH_f=-19.23	Butal2m-2 ΔH_f=-18.43
Butal2m-3 ΔH_f=-9.78	Butal2m-4 ΔH_f=-7.13	Butal2m-5 ΔH_f=-7.13	c4h712ch2oh ΔH_f=-43.02	Butoh2m1d ΔH_f=-50.69
Butoh2m2d ΔH_f=-46.13	Butoh2m3d ΔH_f=-42.83	butoh2m1d3 ΔH_f=-17.19	butoh2m4d3 ΔH_f=-10.03	butoh2m13d ΔH_f=-24.15

Table 3
Ignition delay time correlation parameters in Eq. (1) for *n*-pentanol, *iso*-pentanol and 2-methyl-1-butanol.

Parameters	*n*-Pentanol	*iso*-Pentanol	2-Methyl-1-butanol
$A/10^{-4}$	7.32	2.29	4.29
B	0.419	0.539	0.409
C	0.283	0.388	0.366
D	0.557	0.908	0.778
E_a	34.8	37.7	36.1
Adj. *R*-square	0.993	0.994	0.992

Figure 3a compares the ignition delay time of the three isomers for X_{fuel} = 0.5%, ϕ = 0.5, and *p* = 1.0 atm. In the temperature range investigated herein, τ_{ign} for each isomer increases in the order from *n*-pentanol, 2-methyl-1-butanol, and *iso*-pentanol. However, the disparity in τ_{ign} for these three isomers gradually decreases with increasing temperature. Furthermore, the global activation energy (E_a in Eq. (1)) is the lowest for *n*-pentanol (34.8 kcal/mol) and the highest for *iso*-pentanol (37.7 kcal/mol). Additional comparisons
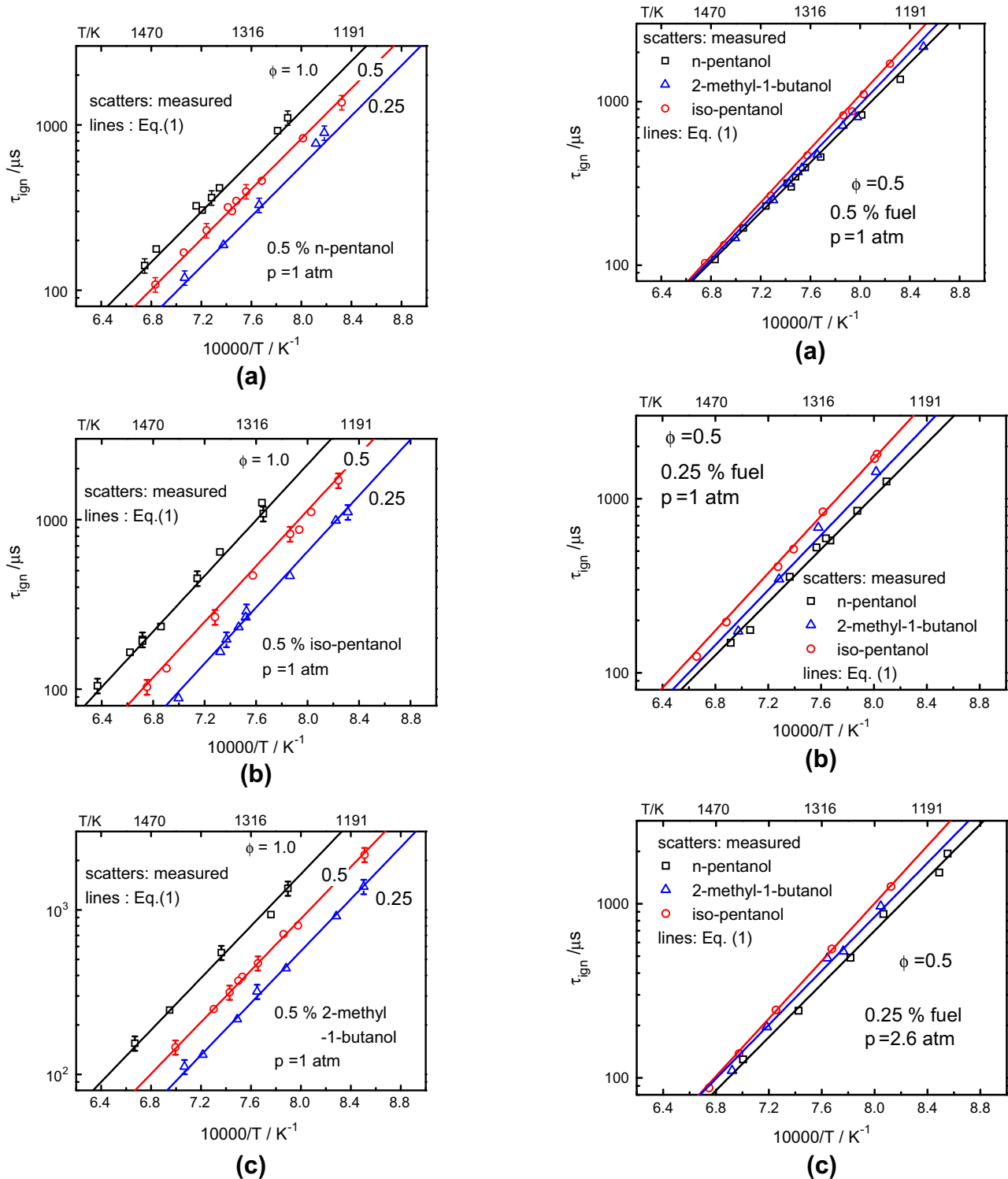

Fig. 2. Ignition delay times for 5% fuel at 1 atm and ϕ = 0.25, 0.5 and 1.0. (a) *n*-Pentanol, (b) *iso*-pentanol and (c) 2-methyl-1-butanol.

Fig. 3. Ignition delay time for three different fuels at ϕ = 0.5. (a) X_{Fuel} = 0.5%, *p* = 1.0 atm, (b) X_{Fuel} = 0.25%, *p* = 1.0 atm, (c) X_{Fuel} = 0.5% and *p* = 2.6 atm.
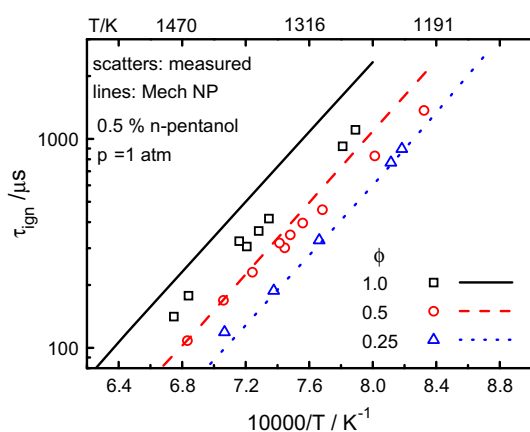
Fig. 4. Comparison between experimental measured and model predicted ignition delay times of n-pentanol for $X_{Fuel} = 0.5\%$, $p = 1.0$ atm and $\phi = 1.0$, 0.5, and 0.25.

(a) iso-pentanol, Mech IP

(b) 2-methyl-1-butanol, Mech 2M1B

Fig. 5. Comparison between experimental measured and predicted ignition delay time for $X_{Fuel} = 0.5\%$, $p = 1.0$ atm and $\phi = 1.0$, 0.5, and 0.25.

of τ_{ign} for the three isomers are made under two other conditions: ($X_{fuel} = 0.25\%$, $\phi = 0.5$, and $p = 1.0$ atm) and ($X_{fuel} = 0.25\%$, $\phi = 0.5$, and $p = 2.6$ atm), respectively shown in Fig. 3b and c. Similar to the trend observed in Fig. 3a, the ignition delay time is the longest for iso-pentanol and shortest for n-pentanol. The relative reactivity of the three pentanol isomers will be discussed in detail at the end of Section 3.4.

3.2. Comparison with numerical computations

The experimental results were compared with calculations using the kinetic mechanism developed by Dagaut and co-workers for n-pentanol [4] (Mech NP) and iso-pentanol [37] (Mech IP), which are the only C5 alcohol mechanisms available.

Figure 4 shows the comparison between the measured and calculated ignition delay times of n-pentanol for three equivalence ratios. Excellent agreement is achieved for $\phi = 0.25$. However, as the equivalence ratio increases, the performance of the model is moderated. In particular, at $\phi = 1.0$, the calculated ignition delay times at 1482 K and 1280 K are respectively 47% and 75% longer than the measured values.

Figure 5a compares the measured and Mech IP predicted ignition delay times of iso-pentanol for three equivalence ratios. Generally, the performance of the model is fairly good, except that in the relatively lower temperature regime, where the model results give an over-prediction (less than 50% for all three equivalence ratios). Figure 5b shows the comparison between the measured and Mech 2M1B predicted ignition delay times of 2-methyl-1-butanol for three equivalence ratios. Similar to the comparisons for iso-pentanol, the Mech 2M1B show good agreement with the measurements for high temperatures and over predicts the ignition delay times at relatively lower temperatures.

We note that the three models only show reasonable performances in predicting the ignition delay times, and further work especially the low temperature chemistry needs to be done by kinetic experts. Thus in the following, we present the sensitivity analysis and reaction pathway flux and hopefully it will be of merits for development of better models.

3.3. Sensitivity analysis

Sensitivity analysis was conducted to identify the reactions that have the strongest impact on the predictions, and hence are appropriate candidates for optimization. The sensitivity coefficient is calculated by perturbing the reaction rate constant, defined as
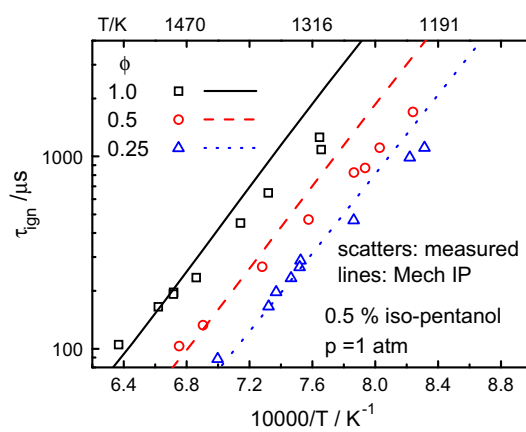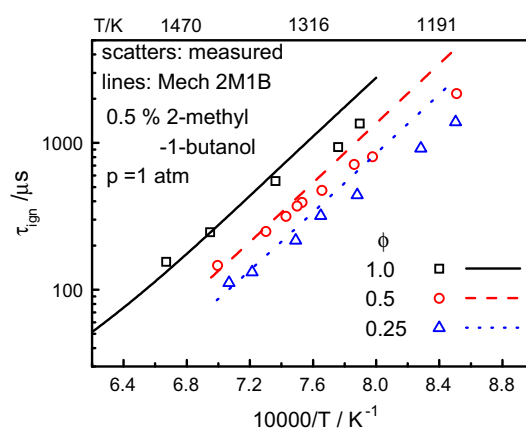
$$S_i = \frac{\Delta \tau_{ign}}{\Delta k_i} \bigg/ \frac{\tau_{ign}}{k_i} \tag{2}$$

where S_i is ignition delay time sensitivity, τ_{ign} ignition delay time, and k_i reaction rate of the ith reaction in mechanism. A negative sensitivity indicates a reduction in τ_{ign}, thus an increase in overall reactivity and vice versa.

In Fig. 6 shows the 15 reactions in Mech NP with the highest sensitivity values for 0.5% n-pentanol, $T = 1350$ K, $p = 1.0$ atm with $\phi = 0.25$ and 1.0. As expected, at this high temperature, the small radical reactions, especially the main chain branching reaction $H + O_2 = OH + O$, dominate the ignition. In addition, reactions associated with the stable species C_3H_6, such as the reverse reaction of $C_3H_6 = C_2H_3 + CH_3$, the three body termination reaction: $aC_3H_5 + H+(M) = C3H6+(M)$, and the OH attack reaction: $C_3H_6 + OH = aC_3H_5 + H_2O$ all consume and/or produce less active radicals thus have the positive sensitivities, leading to reduced reactivity and increased ignition delay time. The only fuel specific reaction among the 15 most sensitive reactions is $eC_5H_{10}OH = cC_3H_6OH + C_2H_4$ because the product of this reaction, C_2H_4, participates in the reaction $C_2H_4 + OH = C_2H_3 + H_2O$ and plays an important role in promoting the reactivity.

Figure 7a presents the 15 most sensitive reactions in Mech IP for 0.5% iso-pentanol, $\phi = 0.5$ and $p = 1.0$ atm. In the temperature range investigated, Mech IP yields good prediction of τ_{ign} at relatively high temperatures but considerable over-estimation at relatively lower temperatures; thus the sensitivities at 1200 K and 1500 K were computed. The results show that the main chain
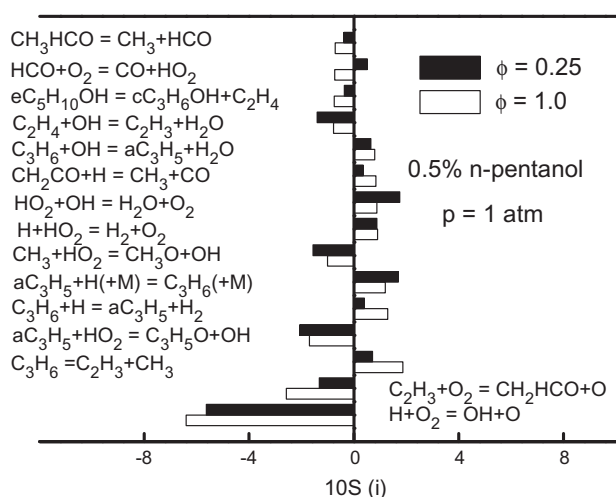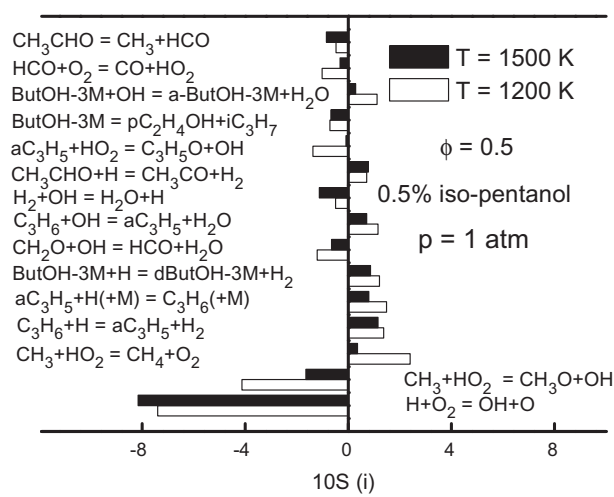
Fig. 6. Ignition delay time sensitivity using Mech NP for 0.5% *n*-pentanol, $T = 1350$ K, $p = 1$ atm, and $\phi = 0.25$ and 1.0.

branching reaction: $H + O_2 = OH + O$ has the largest negative sensitivity. The methyl radical reaction with HO_2 can be facilitating if it is chain branching ($CH_3 + HO_2 = CH_3O + OH$) or inhibiting if it is chain terminating ($CH_3 + HO_2 = CH_4 + O_2$). The most prohibitive fuel specific reactions include the H-abstraction reaction by H from the δ carbon position (relative to the OH group) and by OH from the α carbon position, while the most promoting fuel reaction is the decomposition reaction: But OH-3M = $bC_2H_4OH + i\text{-}C_3H_7$. Figure 7b shows the most sensitive reactions on the ignition delay time prediction of 2-methyl-1-butanol by using Mech 2M1B for 0.5% fuel, $\phi = 0.5$ and $p = 1.0$ atm. Similar to the Mech IP case, the most sensitive promoting reaction is the main chain branching reaction $H + O_2 = O + OH$. The unimolecular decomposition reaction of the fuel promotes the ignition while the H abstraction of the fuel by OH radical is ignition inhibiting.

3.4. Reaction pathway analysis

Figure 8 presents the reaction pathway diagram for *n*-pentanol oxidation, by using Mech NP at the temperature of 1400 K, pressure of 1.0 atm for the stoichiometric mixture with 5% fuel concentration. The diagram illustrates the main destruction channel of *n*-pentanol at the instant of 20% fuel consumption (the *italic* font represents the Mech NP calculation and the black font represents the modified Mech NP). It can be seen that in Mech NP, the fuel is primarily consumed by the unimolecular decomposition and H-abstraction reactions. The unimolecular decomposition, from the first to the last C–C bond breaking, sequentially results in 3.4%, 5%, 5% and 3% fuel consumptions. The H-abstraction reaction is the most prominent fuel consumption channel with total contribution of 74.4%. The H-abstraction from α, β, γ, and δ carbon are equally important with the same 15.5% contribution because in the Mech NP, the reaction rates of the H-abstraction reactions from the α, β, γ, and δ carbon positions were estimated to be the same. H-abstraction from the end carbon consumes 12.4% fuel. In fact, according to the investigation of *n*-butanol oxidation [25], the importance of H-abstraction from different carbon depends on the barrier heights of the H-abstraction reactions. Due to the existence of the OH functional group, H-abstraction from the four different carbon positions of *n*-pentanol should have different branching ratios and the α C–H bond has the lowest bond dissociation energy, thus H-abstraction from the α carbon should have the largest contribution. The fuel radicals generated through H-abstraction then break down through β-scission and isomeriza-

(a)
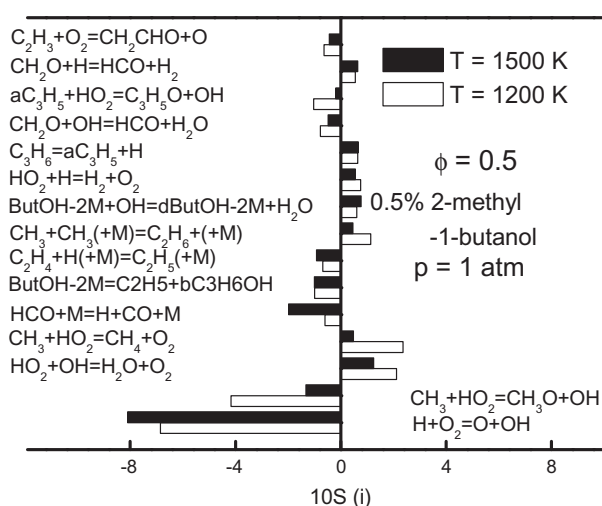
(b)

Fig. 7. Ignition delay time sensitivity of *iso*-pentanol and 2-methyl-1-butanol for $X_{\text{Fuel}} = 0.5\%$, $\phi = 0.5$, $p = 1$ atm, and $T = 1200$ and 1500 K.

tion reactions. Specifically, the $aC_5H_{10}OH$ radical undergoes β-scission reaction to produce nC_3H_7 radical and acetaldehyde. It is noted that in Ref. [43], this reaction initially produces the nC_3H_7 radical and ethenol which partially isomerizes to form acetaldehyde and partially go through decomposition reaction and H-abstraction reactions. The $bC_5H_{10}OH$ radical breaks down through two different pathways of β-scission. One pathway breaks the C–C bond to produce propenol and ethyl radical and the other pathway is elimination of the hydroxyl group. Mech NP shows that these two pathways are nearly equally important (50.1% and 49.9%). The $cC_5H_{10}OH$ can also undergo β-scission through two different pathways. The bond break between the δ and end carbon yields the methyl radical and butenol and accounts for 30.3% fuel radical breakdown and the β-scission through the break of bond between α and β carbon contributes 69.7%. The $dC_5H_{10}OH$ radical primarily isomerizes to produce $aC_5H_{10}OH$ (63.2%) and $C_5H_{11}O$ (28.4%). We expect that there is a β-scission reaction of $dC_5H_{10}OH$ which yields propene and ethanol radical and should contribute a high percentage of the $dC_5H_{10}OH$ breakdown. However, this reaction is not included in Mech NP. The $eC_5H_{10}OH$ radical goes through β-scission and yields ethylene and the propanol radical (50.5%) and isomerization reactions to form $bC_5H_{10}OH$ (40%) and
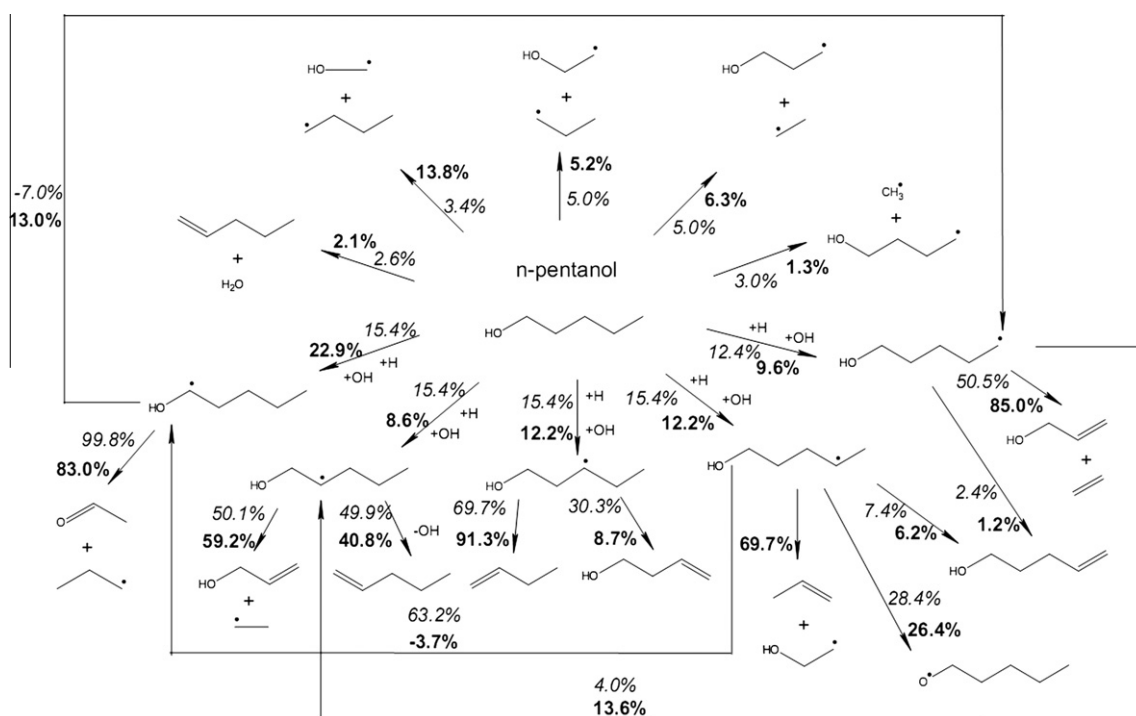
Fig. 8. Reaction pathway diagram of *n*-pentanol oxidation in shock tube at 1400 K for 0.5% *n*-pentanol, $\phi = 1.0$, $p = 1$ atm, at 20% fuel consumption. Black font: Modified Mech NP; Italic fone: Mech NP.

aC5H10OH (7%). It is then speculated that the isomerization reactions of the fuel radical in Mech NP have an over-estimated contribution because β-scission reactions have a much higher rate than isomerization reactions at high temperatures [47]. Evidence can be found for *n*-butanol oxidation in Ref. [25,43], which showed that the isomerization reactions play a very limited role. Thus in Section 3.5, we will present reasonable modifications to the Mech NP.

Figure 9a illustrates the reaction pathway diagram of *iso*-pentanol oxidation in shock tube at 1400 K by using Mech IP for 5% *n*-pentanol, equivalence ratio of 1.0, pressure of 1.0 atm, and at 20% fuel consumption. The model shows that H-abstraction reactions are the most important fuel consumption paths under this condition. Contribution from the end carbon is the most significant (23.3%), followed by the β (21.7%), and α (19.1%) carbon and finally the γ carbon (10.4%). Unimolecular dissociation by breaking of γ-end and β–γ carbon bond respectively contributes 8.0% and 10.7% to the fuel consumption. Unimolecular dissociation reactions from other C–C bond breaking are less important (<3%). The four primary radicals generated from the H-abstraction reactions, namely, butoh3 m-1, butoh3 m-2, butoh3 m-3, and butoh3 m-4 subsequently degenerate to smaller radicals through β-scission reactions. Unlike the oxidation of *n*-pentanol radicals, the four *iso*-pentanol primary radical isomerizations were not found in the reaction pathway diagram because the carbon chain is too short for H atom to be significantly transferred. Figure 9b presents the reaction pathway diagram of 2-methyl-1-butanol at the same condition as in Fig. 9a. Similar to the *iso*-pentanol isomers, 2-methyl-1-butanol is consumed dominantly through H-abstractions (a total of 70.3%) and the produced fuel radicals are primarily decomposed through β scission.

It is noted that Sarathy et al. [43] have discussed the relative reactivity of the butanol isomers and they found that the *tert*-butanol is the least reactive because, compared to *n*-butanol and *iso*-butanol, the unimolecular dehydration is the most significant for *tert*-butanol. However, the unimolecular dehydration is not the reason for the ignition delay time differences for the pentanol isomers studied in Fig. 3 because 2-methyl-1-butanol only has

one available H atom on the β carbon for unimolecular dehydration while either *n*-pentanol or *iso*-pentanol has two and the bond dissociation energies are very equivalent. The results on the reaction fluxes in Figs. 8 and 9 show that all the three isomers are primarily consumed through H-abstraction reactions. Thus it is speculated that the relative reactivity of the three isomers is controlled by different H-abstraction channels resulted from the effects of the branched chain structure. Discussions by Westbrook et al. in Ref. [48] on heptane isomers show that the fuel radicals produced from H-abstractions are dominantly decomposed through β-scission which may finally produce H radicals and promote the ignition through the main chain branching channel: H + O_2 = OH + O, or may produce methyl radical and slow down the ignition through the recombination reaction: CH_3 + CH_3 = C_2H_6. Thus they claimed that the relative reactivity of the heptane isomers depends on the competition between the number of H-abstractions that lead to the H atom production and the number of H-abstractions that lead to the methyl radical production. If we apply the same analysis to the pentanol isomers, we will see that: *n*-pentanol has 2 available H-abstractions (on β carbon) lead to H atom product, and 4 available H-abstractions (2 on α carbon, and 2 on γ carbon) lead to CH_3 radicals; 2-methyl-1-butanol has 2 available H-abstractions (on α carbon) lead to H atom product, and 5 available H-abstractions (2 on α carbon, 1 on β carbon, and 2 on γ carbon) lead to CH_3 radicals; and *iso*-pentanol has 2 available H-abstractions (on α carbon) lead to H atom product, and 8 available H-abstractions (2 on β carbon, and 6 on δ carbon) lead to CH_3 radicals. This analysis explains the difference in the ignition delay times of the three pentanol isomers. Furthermore, as the temperature is increased, the difference among the three isomers is decreased, possibly because the unimolecular decomposition is relatively favored over the H-abstraction reactions when the temperature is increased.

3.5. Analysis of Mech NP

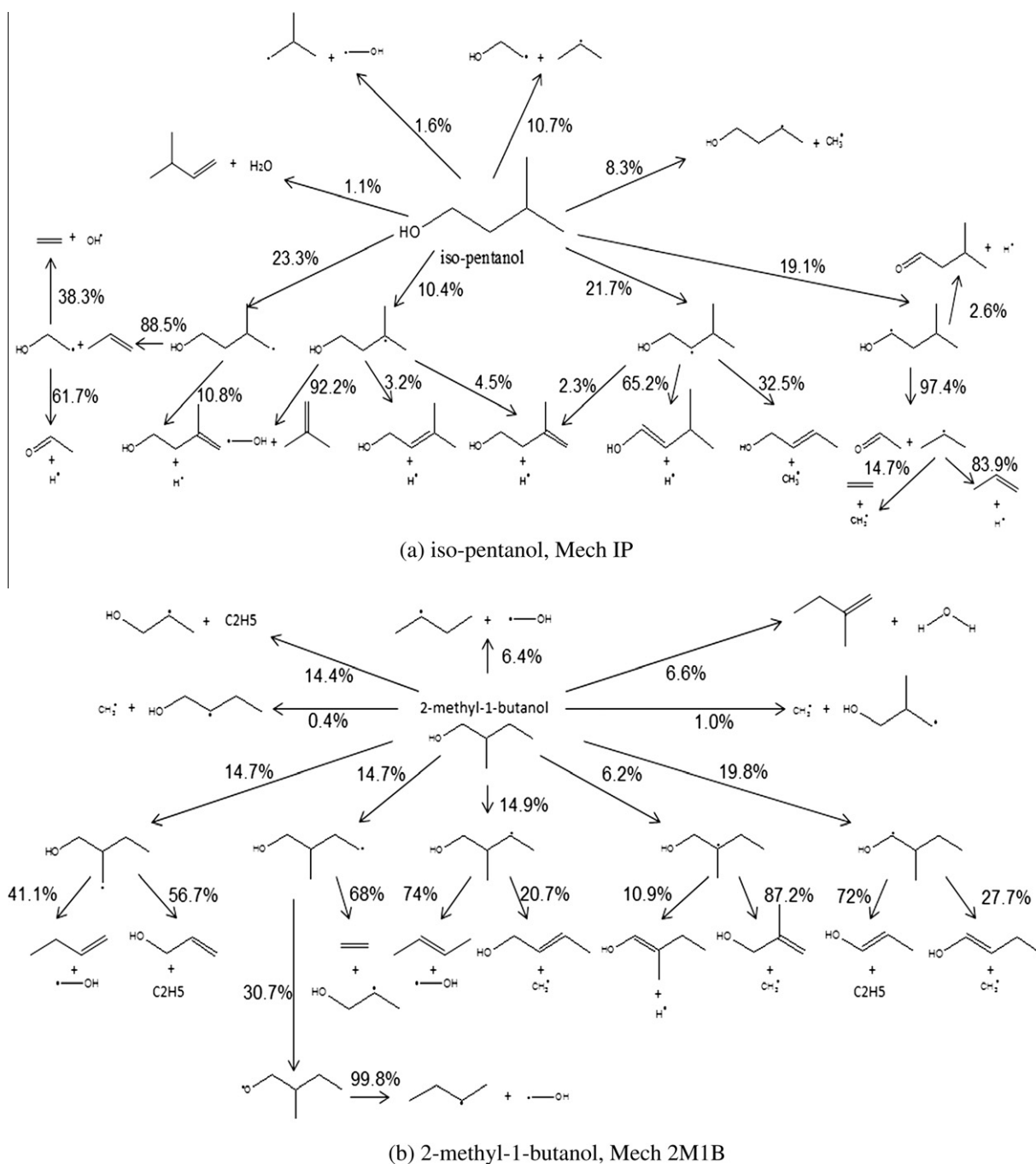We note that the kinetic mechanism of C-5 alcohols has not been much explored and our main objective is to present new

(a) iso-pentanol, Mech IP

(b) 2-methyl-1-butanol, Mech 2M1B

Fig. 9. Reaction pathway diagram of iso-pentanol and 2-methyl-1-butanol oxidation in shock tube at 1400 K for X_{Fuel} = 0.5%, ϕ = 1.0, p = 1 atm, at 20% fuel consumption.

experimental data for subsequent model development. Additionally, the reaction diagram in Section 3.4 shows that there might be some more rational estimation of the *n*-pentanol H-abstraction reactions and the subsequent fuel radical degeneration paths. Furthermore, there is significant disagreement between the Mech NP predictions and experimental measurements for *n*-pentanol ignition delay times under some selected conditions, as shown in Fig. 4. Therefore, *n*-pentanol mechanism needs to be further explored. Moreover, the reaction pathway diagram of *iso*-pentanol in Section 3.4 shows that the sub-mechanism of *iso*-pentanol in Mech IP is more reasonably estimated than that in Mech NP because the rate constants in Mech IP were obtained through rigorous literature review while the rate constants in Mech NP were approximately estimated, as discussed in Section 3.4.

Although the sensitivity analysis in Fig. 6 reveals the dominant role of small radical reactions on ignition, we nevertheless choose to focus on the fuel-specific reactions because their rate constants are much less explored than those of the small radical reactions. A quick scan of Mech NP shows that H atom abstraction reactions by simple species (OH, H, O, etc.) from α, β, γ and δ positions of the fuel have been estimated to have the same rate constants, while recent branching ratio analysis by Zhou et al. [49] for *n*-butanol showed that contributions from the α- and γ-abstractions are significantly higher than those of the β-abstraction, and abstraction from the end carbon (relative to the OH functional group) is strongly temperature sensitive. Thus the rate constants of the H atom abstraction by OH were modified from the analogy of recent published *n*-butanol mechanism [43,44]. Additionally, since there has been
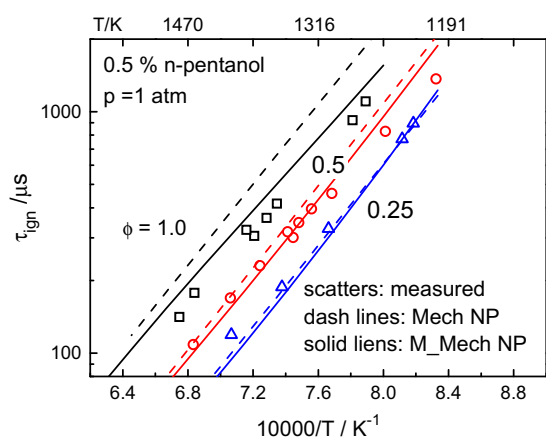
Fig. 10. Comparisons between the Mech NP and M_Mech NP predicted and measured ignition delay times of *n*-pentanol for X_{Fuel} = 0.5%, p = 1.0 atm, ϕ = 1.0, 0.5, 0.25.

from the analogy of a recent *n*-butanol model [29]. As shown in Fig. 8, the modified *n*-pentanol mechanism (black font) has changed the relative importance of the fuel degeneration channels. The added $dC_5H_{10}OH$ decomposition channel (through β scission) contributes 69.7% of this radical decomposition.

Figure 10 shows comparison between the measured and predicted ignition delay times using both Mech NP and the modified mechanism (M_Mech NP). It can be seen that although the modified Mech NP still over-predicts the ignition delay times at ϕ = 1.0, its performance is better than the original Mech NP. Additionally, the jet-stirred reactor results of Ref. [4] are compared with the predictions using Mech NP and the modified Mech NP, as shown in Fig. 11. Results show that all the species concentration profiles computed using the modified Mech NP agree better with the experimental measurements than using the original Mech NP. The improved agreement between the measured and predicted ignition delay times as well as the JSR results indicate that the modifications, though not thorough, can be useful for further mechanism development.

no dehydration reaction in Mech NP, the reaction of *n*-pentanol yielding H_2O and pentene was added in modified Mech NP by employing the rate constants in Ref. [50] from reaction $CH_3CH_2OH = C_2H_4 + H_2O$. Furthermore, for other unimolecular decomposition reactions by simple bond scission, the rate constants are evaluated from the analogy of *n*-butanol in Ref. [51]. Finally, the possibly missed β scission reaction of $dC_5H_{10}OH$ radical was added in the modified Mech NP, and the rate constants were estimated

4. Concluding remarks

Ignition delay times of the three C5 primary alcohol isomers (*n*-pentanol, *iso*-pentanol and 2-methyl-1-butanol) were obtained by using a validated shock-tube facility. Results show that the ignition delay time and global activation energy decrease in the order of *iso*-pentanol, 2-methyl-1-butanol and *n*-pentanol. Available kinetic mechanisms for *n*-pentanol and *iso*-pentanol [37] were used
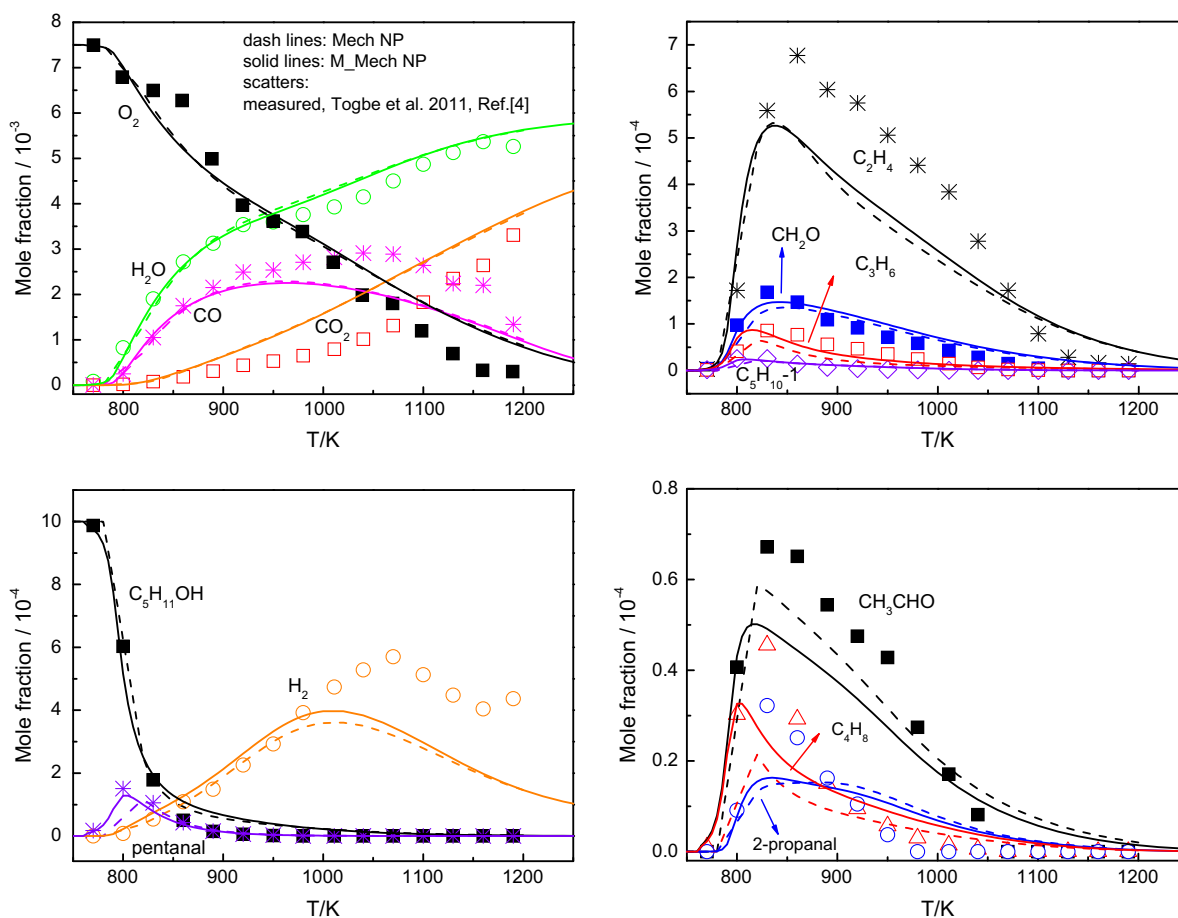

Fig. 11. Predicted species concentrations of measured, Mech NP and Modified Mech NP as function of temperature for *n*-pentanol oxidation in a jet-stirred reactor at ϕ = 1.0, p = 10 atm and τ = 0.7 s.

to model the ignition delay times of *n*-pentanol and *iso*-pentanol, demonstrating that, for *n*-pentanol, the ignition delay times predicted by Mech NP [4] agree well with the measured values at lower equivalence ratio but rather poorly at higher equivalence ratios, while for *iso*-pentanol, the Mech IP [36] slightly under-predicts the ignition delay time at high temperatures but has an over-prediction of 50% at relatively lower temperatures. A 2-methyl-1-butanol mechanism was developed and reasonable agreement with the experimental data was achieved. Sensitivity analysis for all the three isomers reveals the importance of small radical reactions for ignition delay times in the temperature range studied herein. Reaction pathway diagrams were presented to aid the kinetic mechanism analysis and the fuel specific reactions in Mech NP were examined and the rate constants of selected reactions were refined. The modified model yields improved performance on predicting the ignition delay time as well as the JSR results.

Acknowledgments

Appendix A. Supplementary material

Supplementary data associated with this article can be found, in the online version, at http://dx.doi.org/10.1016/j.combustflame.2012.11.018.

References

[1] A. Demirbas, Prog. Energy Combust. Sci. 33 (1) (2007) 1–18.
[2] F. Inal, S.M. Senkan, Combust. Sci. Technol. 174 (9) (2002) 1–19.
[3] R.C. Saxena, D.K. Adhikari, H.B. Goyal, Renew. Sust. Energy Rev. 13 (1) (2009) 167–178.
[4] C. Togbe, F. Halter, F. Foucher, C. Mounaim-Rousselle, P. Dagaut, Proc. Combust. Inst. 33 (2011) 367–374.
[5] B.Q. He, J.X. Wang, X.G. Yan, X. Tian, H. Chen, SAE 2003-01-0762, 2003.
[6] W.D. Hsieh, R.H. Chen, T.L. Wu, T.H. Lin, Atmos. Environ. 36 (3) (2002) 403–410.
[7] S.P. Marshall, S. Taylor, C.R. Stone, T.J. Davies, R.F. Cracknell, Combust. Flame 158 (10) (2011) 1920–1932.
[8] Ömer L. Gülder, Combust. Flame 56 (3) (1984) 261–268.
[9] S. Parag, V. Raghavan, Combust. Flame 156 (5) (2009) 997–1005.
[10] T. Niass, A.A. Amer, W. Xu, S.R. Vogel, K. Krebber-Hortmann, P. Adomeit, A. Brassat, SAE 2011-01-1990, 2011.
[11] J.D. Smith, V. Sick, SAE 2007-01-4034, 2007.
[12] J.R. Wasil, J. Johnson, R. Singh, SAE 2011-01-1197, 2010.
[13] M. Shahbakhti, A. Ghazimirsaied, A. Audet, C.R. Koch, Combustion characteristics of Butanol/n-Heptane blend fuels in an HCCI engine, in: Proceedings of the Combustion Institute-Canadian Section, Spring Technical Meeting, Carleton University, Ottawa, Canada, May 9–12, 2010.
[14] Y. Li, L. Wei, Z. Tian, B. Yang, J. Wang, T. Zhang, F. Qi, Combust. Flame 152 (3) (2008) 336–359.
[15] T. Kasper, P. Oßwald, U. Struckmeier, K. Kohse-Höinghaus, C.A. Taatjes, J. Wang, T.A. Cool, M.E. Law, A. Morel, P.R. Westmoreland, Combust. Flame 156 (6) (2009) 1181–1201.
[16] B. Yang, P. Osswald, Y. Li, J. Wang, L. Wei, Z. Tian, F. Qi, K. Kohse-Hoeinghaus, Combust. Flame 148 (4) (2007) 198–209.
[17] P. Osswald, H. Gueldenberg, K. Kohse-Hoeinghaus, B. Yang, T. Yuan, F. Qi, Combust. Flame 158 (1) (2011) 2–15.
[18] O. Welz, J. Zador, J.D. Savee, M.Y. Ng, G. Meloni, R.X. Fernandes, L. Sheps, B.A. Simmons, T.S. Lee, D.L. Osborn, C.A. Taatjes, Phys. Chem. Chem. Phys. 14 (9) (2012) 3112–3127.
[19] P.S. Veloo, F.N. Egolfopoulos, Proc. Combust. Inst. 33 (2011) 987–993.
[20] W. Liu, A.P. Kelley, C.K. Law, Proc. Combust. Inst. 33 (2011) 995–1002.
[21] X. Gu, Z. Huang, Q. Li, C. Tang, Energy Fuel 23 (2009) 4900–4907.
[22] J.T. Moss, A.M. Berkowitz, M.A. Oehlschlaeger, J. Biet, V.r. Warth, P.-A. Glaude, F.d.r. Battin-Leclerc, J. Phys. Chem. A 112 (43) (2008) 10843–10855.
[23] M.V. Johnson, S.S. Goldsborough, Z. Serinyel, P. O'Toole, E. Larkin, G. O'Malley, H.J. Curran, Energy Fuel 23 (12) (2009) 5886–5898.
[24] I. Stranic, D.P. Chase, J.T. Harmon, S. Yang, D.F. Davidson, R.K. Hanson, Combust. Flame 159 (2) (2011) 516–527.
[25] G. Black, H.J. Curran, S. Pichon, J.M. Simmie, V. Zhukov, Combust. Flame 157 (2) (2010) 363–373.
[26] K.A. Heufer, R.X. Fernandes, H. Olivier, J. Beeckmann, O. Roehl, N. Peters, Proc. Combust. Inst. 33 (2011) 359–366.
[27] K.E. Noorani, B. Akih-Kumgeh, J.M. Bergthorson, Energy Fuel 24 (11) (2010) 5834–5843.
[28] T.S. Norton, F.L. Dryer, Proc. Combust. Inst. 23 (1) (1991) 179–185.
[29] S.M. Sarathy, M.J. Thomson, C. Togbe, P. Dagaut, F. Halter, C. Mounaim-Rousselle, Combust. Flame 156 (4) (2009) 852–864.
[30] P. Dagaut, S.M. Sarathy, M.J. Thomson, Proc. Combust. Inst. 32 (1) (2009) 229–237.
[31] J.K. Lefkowitz, J.S. Heyne, S.H. Won, S. Dooley, H.H. Kim, F.M. Haas, S. Jahangirian, F.L. Dryer, Y. Ju, Combust. Flame 159 (3) (2012) 968–978.
[32] A.F. Cann, J.C. Liao, Appl. Microbiol. Biotechnol. 85 (4) (2010) 893–899.
[33] H.-C. Tseng, Production of Pentanol in Metabolically Engineered Escherichia Coli, Massachusetts Institute of Technology, Massachusetts, 2011.
[34] S. Atsumi, T. Hanai, J.C. Liao, Nature 451 (7174) (2008) 86–89.
[35] Y. Yang, J. Dec, N. Dronniou, B. Simmons, SAE 2010-01-2164, 2010.
[36] T. Tsujimura, W.J. Pitz, Y. Yang, J.E. Dec, SAE 2011-24-0023, 2011.
[37] G. Dayma, C. Togbé, P. Dagaut, Energy Fuel 25 (11) (2011) 4986–4998.
[38] Y. Zhang, Z. Huang, L. Wei, J. Zhang, C.K. Law, Combust. Flame 159 (3) (2012) 918–931.
[39] A. Burcat, B. Ruscic. Third Millennium Ideal Gas and Condensed Phase Thermochemical Database for Combustion with Updates from Active Thermochemical Tables. <http://garfield.chem.elte.hu/Burcat/burcat.html>.
[40] E.R. Ritter, J.W. Bozzelli, Int. J. Chem. Kinet. 23 (9) (1991) 767–778.
[41] S.W. Benson, F.R. Cruickshank, D.M. Golden, G.R. Haugen, H.E. O'Neal, A.S. Rodgers, R. Shaw, R. Walsh, Chem. Rev. 69 (3) (1969) 279–324.
[42] J. Zhang, L. Wei, X. Man, X. Jiang, Y. Zhang, E. Hu, Z. Huang, Energy Fuel 26 (6) (2012) 3368–3380.
[43] S.M. Sarathy, S. Vranckx, K. Yasunaga, M. Mehl, P. Oßwald, W.K. Metcalfe, C.K. Westbrook, W.J. Pitz, K. Kohse-Höinghaus, R.X. Fernandes, H.J. Curran, Combust. Flame 159 (6) (2012) 2028–2055.
[44] K. Yasunaga, T. Mikajiri, S.M. Sarathy, T. Koike, F. Gillespie, T. Nagy, J.M. Simmie, H.J. Curran, Combust. Flame 159 (6) (2012) 2009–2027.
[45] J.P. Orme, H.J. Curran, J.M. Simmie, J. Phys. Chem. A 110 (1) (2006) 114–131.
[46] W.H. Green, Reaction Mechanism Generator, <http://rmg.coe.neu.edu/>.
[47] R. Grana, A. Frassoldati, T. Faravelli, U. Niemann, E. Ranzi, R. Seiser, R. Cattolica, K. Seshadri, Combust. Flame 157 (11) (2010) 2137–2154.
[48] C.K. Westbrook, W.J. Pitz, H.C. Curran, J. Boercker, E. Kunrath, Int. J. Chem. Kinet. 33 (12) (2001) 868–877.
[49] C.W. Zhou, J.M. Simmie, H.J. Curran, Combust. Flame 158 (4) (2011) 726–731.
[50] R. Sivaramakrishnan, M.C. Su, J.V. Michael, S.J. Klippenstein, L.B. Harding, B. Ruscic, J. Phys. Chem. A 114 (35) (2010) 9425–9439.
[51] P.S. Veloo, Y.L. Wang, F.N. Egolfopoulos, C.K. Westbrook, Combust. Flame 157 (10) (2010) 1989–2004.